Two-component protein-engineered physical hydrogels for cell encapsulation

Cheryl T. S. Wong Po Foo[a], Ji Seok Lee[a], Widya Mulyasasmita[b], Andreina Parisi-Amon[b], and Sarah C. Heilshorn[a,1]

[a]Materials Science and Engineering and [b]Bioengineering, Stanford University, 476 Lomita Mall, Stanford, CA 94305

Edited by David A. Tirrell, California Institute of Technology, Pasadena, CA, and approved October 13, 2009 (received for review May 1, 2009)

Current protocols to encapsulate cells within physical hydrogels require substantial changes in environmental conditions (pH, temperature, or ionic strength) to initiate gelation. These conditions can be detrimental to cells and are often difficult to reproduce, therefore complicating their use in clinical settings. We report the development of a two-component, molecular-recognition gelation strategy that enables cell encapsulation without environmental triggers. Instead, the two components, which contain multiple repeats of WW and proline-rich peptide domains, undergo a sol–gel phase transition upon simple mixing and hetero-assembly of the peptide domains. We term these materials mixing-induced, two-component hydrogels. Our results demonstrate use of the WW and proline-rich domains in protein-engineered materials and expand the library of peptides successfully designed into engineered proteins. Because both of these association domains are normally found intracellularly, their molecular recognition is not disrupted by the presence of additional biomolecules in the extracellular milieu, thereby enabling reproducible encapsulation of multiple cell types, including PC-12 neuronal-like cells, human umbilical vein endothelial cells, and murine adult neural stem cells. Precise variations in the molecular-level design of the two components including (*i*) the frequency of repeated association domains per chain and (*ii*) the association energy between domains enable tailoring of the hydrogel viscoelasticity to achieve plateau shear moduli ranging from ≈9 to 50 Pa. Because of the transient physical crosslinks that form between association domains, these hydrogels are shear-thinning, injectable, and self-healing. Neural stem cells encapsulated in the hydrogels form stable three-dimensional cultures that continue to self-renew, differentiate, and sprout extended neurites.

biomaterial | cell transplantation | protein engineering

Hydrogels are ideal materials for implantation because they introduce low levels of foreign matter into the body and allow high diffusivity of biomolecules (1). Hydrogel crosslinks can be either chemical (2–4) or physical (5–7). Because many chemical crosslinkers are toxic and result in noninjectable gels, physical hydrogels are preferred for many biomedical applications. Many physical hydrogels are shear-thinning and injectable, an important criterion for noninvasive cell and drug delivery. However, the assembly of polymers into physical hydrogels for cell encapsulation has been governed mostly by the use of external triggers (5, 8–11). In these systems, cells are mixed with precursors in the solution phase then exposed to a change in pH, temperature, or ionic concentration to induce a gel phase transition. Common triggers include temperature sweeps from 4 to 37 °C for collagen (12) and Matrigel (13), pH shifts from ≈2.5 to 7.4 for PuraMatrix (13) and leucine-zipper systems (5), and cation concentration increases from 20 to 200 mM for alginate (12, 14) and peptide amphiphiles (8).

These materials are designed generally to be gels at physiological conditions, requiring that cells be exposed momentarily to nonideal environmental conditions in the solution phase. Because cells are highly sensitive to these nonphysiological conditions, these triggers can be irreversibly detrimental to the encapsulated cells and accompanying proteins; furthermore, these environmental conditions can be difficult to reproducibly control in clinical settings (15). Current cell injection techniques can result in substantial loss of transplanted viable cells (16, 17). This is important because cell viability directly correlates to the success of cell transplantation therapies (18). In response, we use the concept of protein–protein interactions between specific peptide domains to design a two-component, molecular-recognition physical hydrogel. The two components contain separate peptide domains that associate upon mixing under constant physiological conditions (Fig. 1). Therefore, this two-component hetero-assembly strategy is tailor-made to encapsulate cells and proteins without subjecting them to variations in pH, temperature, or ionic strength. We term these materials mixing-induced, two-component hydrogels (MITCHs).

Three criteria were used to select the association domains for our engineered proteins. First, their amino acid sequences must be short to allow multiple domains to be repeated in a single polymer that expresses well in a recombinant host. Second, the domains must be found naturally intracellularly so as not to interfere with external cell signaling when presented as part of a hydrogel matrix. Third, the domain association should be specific and tunable. The WW domain and the proline-rich peptide, two small peptide domains that associate together, were found to meet these criteria. The WW domains, so named because of their conserved tryptophan residues (single-letter amino acid symbol: W) within the consensus sequence, fold into antiparallel β-sheet structures (19). Many variants of this well-studied structure are found in multiple intracellular proteins, and further variants have been derived computationally (20–23). Therefore, the WW domain and the proline-rich peptide represent a large library of potential association domains with varying degrees of binding specificity and strength. Multiple repeats of each association domain were linked together with random-coil hydrophilic spacers to form three separate families of engineered recombinant proteins with varying chain lengths (Fig. 1 and Fig. S1*a*). These block copolymers are synthesized using recombinant protein engineering, which requires complete specification of the primary amino acid sequence. Here, we demonstrate how this sequence control can be used to precisely dictate the association domain frequency (i.e., number of repeats per chain) and binding affinity (K_d), thereby tailoring the MITCH bulk rheological properties via molecular-level design.

This design strategy is unique in two ways from previous work using physical crosslinks to induce the hetero-assembly of two-component hydrogels (7). First, many reported two-component hydrogel systems rely on interactions that are difficult to tailor at constant physiological conditions. For example, the stereo-

Author contributions: C.T.S.W.P.F. and S.C.H. designed research; C.T.S.W.P.F., J.S.L., W.M., and A.P.-A. performed research; C.T.S.W.P.F., J.S.L., W.M., A.P.-A., and S.C.H. analyzed data; and C.T.S.W.P.F. and S.C.H. wrote the paper.

The authors declare no conflict of interest.

This article is a PNAS Direct Submission.

Freely available online through the PNAS open access option.

[1]To whom correspondence should be addressed. E-mail: heilshorn@stanford.edu.

This article contains supporting information online at www.pnas.org/cgi/content/full/0904851106/DCSupplemental.

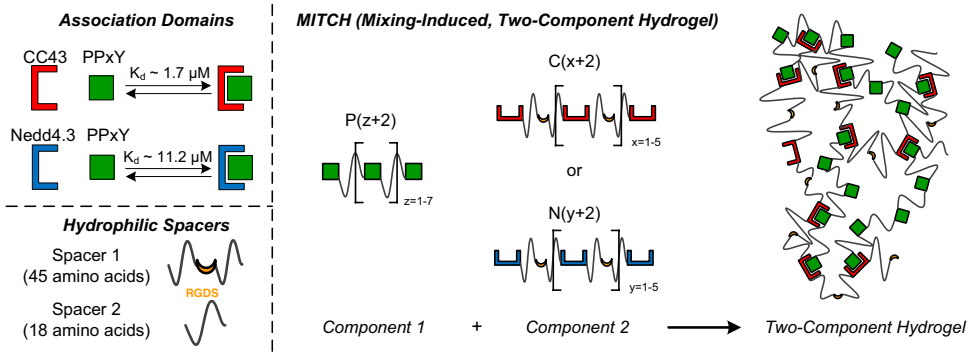

Fig. 1. Schematic of the mixing-induced, two-component hydrogel. (*Top left*) Modular association domains assemble via molecular recognition. Two WW domains (CC43 and a Nedd4.3 variant) bind the same proline peptide (PPxY). (*Bottom left*) Hydrophilic spacers link multiple repeats of WW domains (spacer 1) or proline peptides (spacer 2). Spacer 1 contains a cell-adhesion peptide RGDS. (*Right*) Three engineered protein families: C[$x + 2$], N[$y + 2$], and P[$z + 2$]. Mixing component 1 with component 2 (either C[$x + 2$] or N[$y + 2$]) at constant physiological conditions results in hydrogel formation.

complexation of enantiomers of polylactic acid (24, 25) and the interaction of β-cyclodextrin polymers with various complementary guest molecules (26, 27) have been explored as controlled-release hydrogels. Because of the relative nonspecificity of these interactions compared with peptide–peptide associations, tuning the association energy between the two polymers at constant physiological conditions can be somewhat difficult for cell encapsulation applications. Second, previous peptide-based two-component hydrogels were designed to interact with specific molecules in the extracellular environment for particular applications, including delivery of growth factors (28), display of heparin-binding peptides (29), and sensing of calcium ions (30). In contrast, we have chosen association domains that normally are not present in the extracellular environment; therefore, our materials are engineered to be noninteractive with the extracellular milieu for specific applications in cell encapsulation, which requires reproducible hydrogel formation even in the presence of additional biomolecules. Because of their ease of use, tunability, and reproducibility, these MITCH materials may be applicable to a wide range of potential cell injection therapies.

A variety of new cell injection protocols are currently under investigation for treatment of a myriad of diseases and injuries (17, 31–34). Here, we focus on potential applications in the central nervous system. Unlike many other tissues, the adult central nervous system has a limited capacity for self-repair (35). Transplantation of many cell types including endothelial cells (36) and adult neural stem cells (37) have produced partial functional recovery in animal models with a wide spectrum of lesions. However, most cell transplantation protocols inject cells suspended in liquid medium, which often results in low viability after implantation (15–35%) and unpredictable outcomes (38–40). Cell viability directly correlates to functional outcome; therefore, there is a strong need to develop efficient methods of cell delivery (41, 42). As a first step toward this goal, we demonstrate that our MITCH system can encapsulate endothelial and neural stem cells successfully, maintain cellular proliferation, and support cellular differentiation and three-dimensional cell spreading.

Results

Engineered Protein Design, Synthesis, and Characterization. The MITCH polymers were designed using protein engineering concepts and simple polymer physics considerations. The WW domain (≈31–40 aa) has shown surprising specificity and affinity for proline-rich peptides despite its nonconserved sequences (20). Many WW domain sequences have been identified in nature and derived computationally (21–23). For our studies, we chose two WW domains, the computationally derived CC43 (22) and a slight variation of the wild-type sequence Nedd4.3 (21, 22), reported to differ by an order of magnitude in their association constants with group I proline-rich peptides (PPxY). The hydrophilic spacers were hypothesized to add flexibility to the protein chains, thereby facilitating accessibility and binding between the WW and PPxY domains. We designed the length of hydrophilic spacer 1, which links multiple WW domains, to be equal to or greater than the length of a single WW domain [≈25 Å based on X-ray crystallography (43)] assuming that the spacer has a self-avoiding random-coil configuration (5, 44). The length of hydrophilic spacer 2, which links multiple PPxY domains, was chosen to be a non-integer multiple (2/5) of spacer 1 to minimize the possibility of several physical crosslinks forming between a single component 1 chain and a single component 2 chain (i.e., "zipping up" of pairs of molecules), which would prevent the formation of a fully linked network.

The synthesis of these precisely designed polymers was achieved by using recombinant protein technology to encode each primary sequence in an exact modular genetic construct (Fig. S1*b*). The engineered proteins were expressed in *Escherichia coli*, purified via affinity chromatography, and characterized by gel electrophoresis, mass spectrometry, and amino acid composition analysis (Fig. S2). To verify that the association domains properly fold and bind when fused to hydrophilic spacers on their C and N termini, secondary structure and binding analyses were performed on protein polymers with three repeats of each domain (C3, N3, and P3). Circular dichroism of C3 and N3 showed the characteristic features associated with the antiparallel, triple-stranded β-sheet fold of a WW domain (19) (Fig. S3). Binding affinities were measured by isothermal titration calorimetry and tryptophan fluorescence quenching experiments (Fig. S3). P3 binds to C3 and N3 with apparent dissociation constants of 4.6 ± 0.01 μM and 62 ± 4.6 μM, respectively, consistent with previous observations of monomeric units of CC43 and Nedd4.3 bound to a model group I polyproline peptide (apparent dissociation constants of 1.7 ± 0.1 μM and 11.2 ± 1.2 μM, respectively) (22) (Fig. S3). These assays demonstrate that the modular approach to protein engineering allows for the systematic design of families of proteins that physically bind through precise molecular-recognition interactions with tunable association energies.

Microrheology and Bulk Rheology of Protein-Engineered Hydrogels. The rheological properties first were evaluated using microrheology, where the Brownian motion trajectories of micrometer-sized fluorospheres embedded within the solutions are tracked over time (26, 45, 46). On the time scale of these experiments, all of the individual component solutions (7.5 wt %) appear to

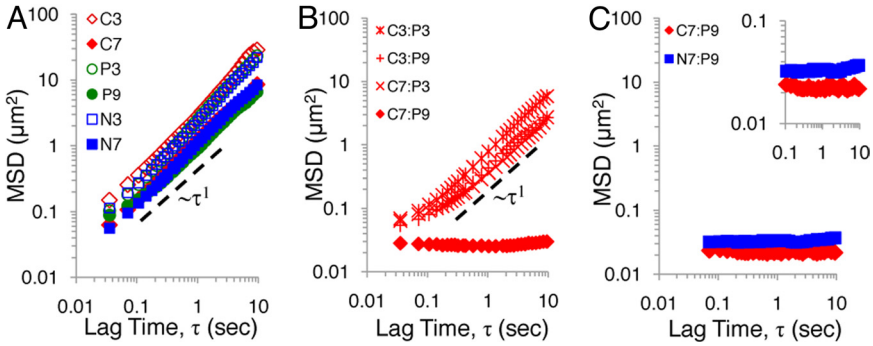

Fig. 2. Microrheological characterization. (*A*) Mean-squared displacement (MSD) of fluorospheres embedded within solutions of C3, C7, N3, N7, P3, and P9 (7.5 wt %). Dashed line indicates MSD power-law scaling of τ^1. (*B*) Mean-squared displacement of mixed solutions of C3:P3, C7:P3, C3:P9, and C7:P9 (7.5 wt %). (*C*) Mean-squared displacement of mixed solutions of C7:P9 and N7:P9 (7.5 wt %).

behave as viscous Newtonian fluids, because the mean-squared displacement (MSD) of the particles scales linearly with time, τ (Fig. 2*A*) (45). As expected, MSD for the higher molecular weight polymers (C7, P9, and N7) is less than that of the lower molecular weight polymers (C3, P3, and N3), because of an increase in solution viscosity.

Transient physical crosslinks are formed between adjacent polymers by mixing together solutions that contain the C and P domains. The probability of forming a crosslink, p, times the functionality, f (i.e., number of potential crosslinking sites per chain), gives the average number of crosslinks formed per chain. To form a stable hydrogel network, the crosslink probability, p, must be above the gel-point threshold, p_c. In mean-field treatments of gelation, the gel-point threshold to induce the formation of a percolating polymeric network, p_c, decreases as the functionality, f, is increased (47–49). To examine the role of functionality in this MITCH system, solutions of polymers with varying numbers of repeated association domains per chain, f, were made with identical weight per volume concentrations (7.5 wt %); thus, the total number of potential crosslinks within each mixture is identical. The microrheological measurements demonstrate a clear difference in MSD behavior for the highest functionality C7:P9 mixture compared with the lower functionality combinations of C3:P3, C3:P9, and C7:P3 (Fig. 2*B*). Although at short time scales the low functionality mixtures exhibit subdiffusive particle behavior indicative of viscoelasticity, ultimately the particle trajectories trend toward τ^1 at time scales >1 s, indicating liquid-like behavior. These data are consistent with visual observations that the mixtures are freely flowing solutions. In contrast, MSD in the C7:P9 mixture was found to be nearly independent of time across the range of time scales observed, indicative of the formation of a hydrogel network and consistent with visual observations of the gel-phase transition (Fig. S4). Therefore, altering the number of repeated association domains included in each chain enables direct manipulation of the viscoelastic properties by tuning of the gel-point threshold.

Although the ideal viscoelastic properties of hydrogels for cell transplantation are not yet well understood, the gel should result in uniform cell suspensions (9). Additionally, because cell morphology, adhesion, differentiation, and gene expression can be altered in response to biomechanical cues (50–52), the ability to systematically tune the hydrogel viscoelasticity is critical. We hypothesized that our modular design strategy would allow systematic control over the viscoelasticity not only through variation of the frequency but also through variation of the binding affinity. As expected, substituting the weaker binding N7 component for the stronger binding C7 component resulted in hydrogels with significantly higher MSD values, indicative of more compliant gels (Fig. 2*C*). Furthermore, viscoelasticity also was tuned by altering the protein concentration of the mixtures (Fig. S4). These results demonstrate that judicious selection of the molecular-level peptide building blocks can be used to predictably tune the macroscopic hydrogel viscoelastic properties.

Although microrheology data can be used to directly compute frequency-dependent storage (G') and loss (G'') moduli, these transformations presume correct knowledge of the MSD behavior across an infinite range of time scales; therefore, large errors can be introduced commonly in these calculations (53). To avoid this, bulk rheology was used to determine G' and G'' behavior of the hydrogels (10 wt %). Within the linear viscoelastic range of both mixtures, the plateau G' was larger than G'', indicative of the gel phase (Fig. S4). At room temperature, C7:P9 has a G' value of ≈50 Pa, similar to 100% Matrigel, whereas the weaker binding N7:P9 has a G' value of ≈9 Pa, similar to 50% Matrigel (54). Matrigel is a commercially available hydrogel commonly used for cell encapsulation and transplantation preclinical studies. However, because of its isolation from the basement membrane of a mouse sarcoma, Matrigel is unlikely to be approved for clinical use (16, 17). These data demonstrate that the viscoelastic properties exhibited by the MITCH materials are within the appropriate range for cell encapsulation and transplantation applications.

Because these hydrogels are formed by weak, transient crosslinks, we hypothesized that they would be shear-thinning, injectable, and self-healing, which are desirable properties for potential clinical materials (10, 16, 17). We ejected fully formed C7:P9 and N7:P9 gels (7.5 wt %) through a 26-gauge syringe needle (commonly used for patient insulin injections) by hand into microrheology chambers. The MSD behavior of the shear-thinned samples was monitored during the self-healing process until a fully formed hydrogel with viscoelastic properties identical to that of the presheared gel was achieved (Fig. 3). For the stronger binding C7:P9, complete self-healing occurred in 5 min; in contrast, the weaker binding N7:P9 required 30 min to self-heal. These results demonstrate that the MITCH materials are candidates for use as clinically injectable hydrogels and that molecular-level design of the polymers can tailor the kinetics of self-healing.

Protein-Engineered Hydrogels Support Three-Dimensional Cell Culture. The bioactivity and biocompatibility of the MITCH materials were assessed initially on two-dimensional (2D) films of the C7:P9 and N7:P9 hydrogels using a neuronal-like PC-12 cell line and dissociated murine adult neural stem cells (NSCs). We incorporated biofunctionality into the hydrogels by introducing a fibronectin-derived RGDS cell-adhesion sequence within hydrophilic spacer 1 (Fig. 1 and Fig. S1*a*). PC-12 cell proliferation on C7:P9 and N7:P9 gels, as monitored by DNA quantification, was comparable to that on a positive control collagen I substrate and enhanced over noncoated tissue culture plastic, a common

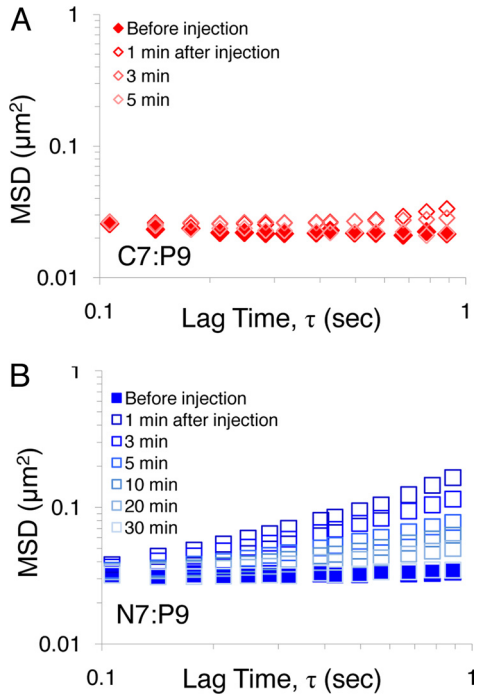

Fig. 3. Hydrogel shear-thinning and self-healing. Mean-squared displacement (MSD) of (*A*) C7:P9 and (*B*) N7:P9 gels (7.5 wt %) before and at multiple times after shear-thinning through a syringe needle.

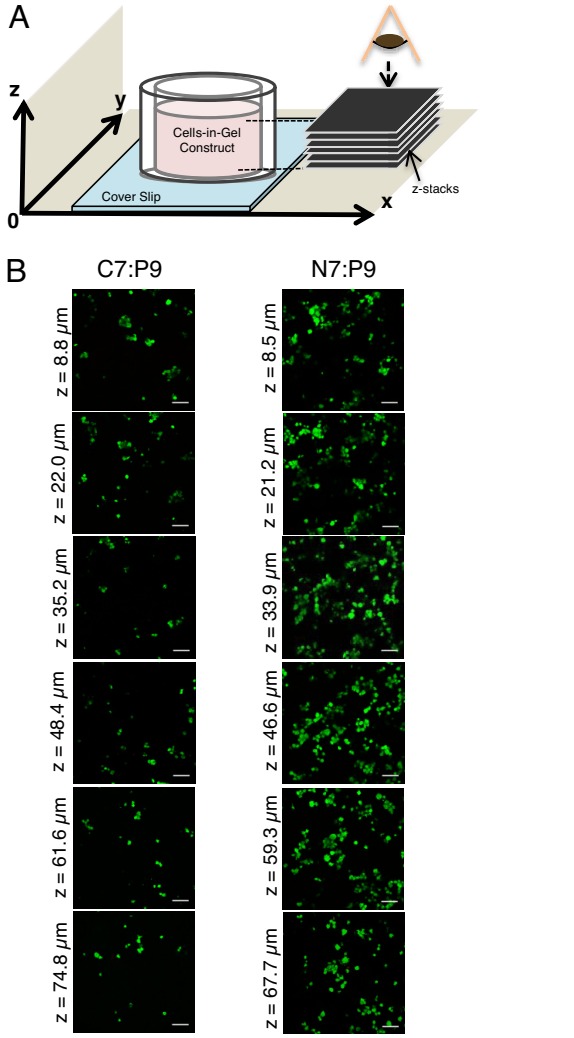

Fig. 4. Encapsulated human umbilical vein endothelial cells. (*A*) Viewing orientation relative to the cell–gel mixture. (*B*) Confocal *z*-plane micrographs of viable (green, calcein AM) and dead (red, ethidium homodimer) cells, indicating dispersion throughout C7:P9 and N7:P9 gels (7.5 wt %). (Scale bars, 50 μm.)

negative control for adherent PC-12 cells (55) (Fig. S5). For NSCs, which do not require substrate adhesion, DNA quantification on all of the substrates was similar (56) (Fig. S5). Additionally, NSCs grown on C7:P9 and N7:P9 hydrogel films were able to self-renew and maintain their neural multipotency as observed via nestin-positive immunocytochemistry when cultured in proliferation medium (Fig. S5). Cultures of PC-12 cells and NSCs on C7:P9 and N7:P9 gels adopted typical neural morphologies after differentiation, with PC-12 cells showing long neuronal extensions (Fig. S5) and NSCs displaying glial (GFAP-positive) and neuronal (MAP2-positive) phenotypes (Fig. S5).

To encapsulate cells within three-dimensional (3D) gels at constant physiological conditions, cells were premixed with solutions of C7 or N7 before the addition of P9 to induce gelation (Fig. S6). Microrheology confirmed that the molecular recognition between WW and proline-rich peptide domains was not disrupted by the presence of biomolecules in the culture medium, including 5% FCS (Fig. S7). Three cell culture types were evaluated in 3D encapsulation studies: PC-12 cells as a reproducible model cell line, human umbilical vein endothelial cells (HUVECs) as a clinically relevant human cell type (36), and murine adult NSCs as cells used in animal models of central nervous system regeneration (37). After encapsulation, *z*-stack confocal imaging of calcein-AM-labeled living cells and ethidium-homodimer-labeled dead cells showed highly viable cells distributed throughout the gels (Fig. 4 and Fig. S8). The relatively uniform cell distributions in both gels confirm the visually observed fast gelation kinetics, which form in ≈30 s, consistent with previous peptide assembly studies that reported decreasing the gelation time from 1 h to 40 s resulted in homogeneous distributions of cells (9, 57). Both suspensions of single cells (Fig. S8 *a* and *b*) and suspensions of larger NSC neurosphere aggregates (Fig. S8 *c* and *d*) were viable and stable after 5 days of 3D culture. Together, the results from the HUVEC, PC-12, and NSC studies demonstrate the cytocompatibility and ease of use of these MITCH materials for a potentially wide range of cell encapsulation applications.

Finally, to demonstrate that MITCH materials could support the differentiation of adult NSCs in 3D culture, encapsulated cell–gel mixtures were exposed to a 6-day differentiation protocol. Neuronal MAP2-positive and glial GFAP-positive cells were present in both C7:P9 and N7:P9 gels, whereas no nestin-positive cells were observed in any of the samples after differentiation (Fig. 5). Multiple elongated neurites, often extending >100 μm in length in all three directions, were observed. These data demonstrate that our gels can support the self-renewal, differentiation, and elongated neurite extension of NSCs in 3D cultures.

Discussion

These results demonstrate an effective strategy to encapsulate cells within injectable physical hydrogels. Gelation is based solely on the cumulative effects of specific molecular-recognition interactions between WW domains and proline-rich peptides repeated within the sequences of two distinct engineered components. This is the first demonstrated use of WW and proline-rich peptide domains in protein-engineered materials. A wide

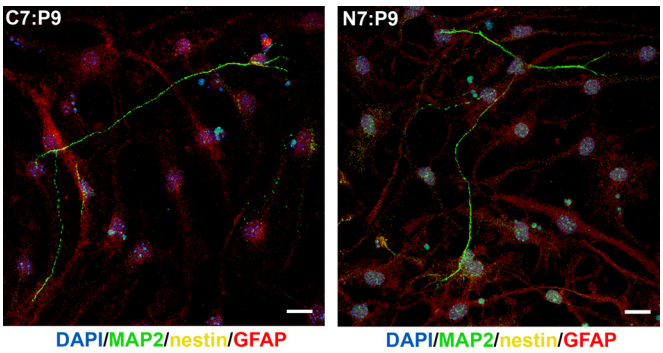

Fig. 5. Encapsulated adult neural stem cell differentiation. Confocal *z*-stack projections of NSCs differentiated within C7:P9 and N7:P9 gels (5 wt %) at 6 days (red, glial marker GFAP; green, neuronal marker MAP2; yellow, progenitor marker nestin; blue, nuclei, DAPI). (Scale bars, 25 μm.)

variety of WW domains with varying binding affinities for specific proline-rich peptide sequences have been reported in the literature; therefore, this work greatly expands the library of potential peptide domains that can be incorporated successfully into protein-engineered materials.

This MITCH strategy allows simple and gentle cell encapsulation without compromising cell viability and without the use of any environmental triggers. Because WW and proline-rich peptide domains are found generally in intracellular proteins, the hetero-assembly of these domains is not disrupted by the presence of additional biomolecules in the extracellular milieu. The fast gelation kinetics observed allow for cell distribution throughout the gel. In addition, the shear-thinning, injectability, and self-healing properties of the MITCH materials make them attractive candidates for potential cell injection applications. Currently, we are using a dorsal subcutaneous mouse model (16) to monitor the viability and distribution of cells delivered via injection within MITCH materials.

The synthetic accuracy of protein engineering allows both components of the MITCH material to be modified precisely. We have demonstrated that two molecular-level design parameters (*i*) the frequency of association domains and (*ii*) the binding strength between association domains can fine-tune the hydrogel viscoelasticity. In addition to these two molecular-level variables, we hypothesize that tailoring the length of the hydrophilic spacers linking together multiple association domains also will result in altered hydrogel viscoelasticity. Therefore, the biosynthetic strategy used here will enable the further design of additional MITCH polymers with precisely tailored molecular parameters, which may provide future insights into the relationship among molecular-level design, mesoscale network structure, and macroscopic hydrogel properties.

The protein engineering biosynthetic strategy also enabled the incorporation of the cell-adhesive RGDS peptide directly into the backbone of the MITCH materials at precise locations. These cell-adhesive materials supported the 3D culture and proliferation of PC-12 cells, HUVECs, and NSCs. Although recent studies have demonstrated that 2D NSC cultures were unable to self-renew or differentiate on top of substrates with moduli of ≈10 Pa, our data demonstrate that weak hydrogels (G' ≈ 9–50 Pa) support the self-renewal, differentiation, and elongated neurite extension of NSCs in 3D (58). These results suggest that the range of mechanical properties that elicit specific cellular responses may be different in 2D versus 3D, similar to recent reports of dimensionality effects on the biomechanics of endothelial cells (59, 60). Because of their highly tunable nature and precise synthetic strategy, these MITCH materials may be well suited to probe these types of biomechanical and biochemical effects on 3D in vitro cultures. For example, through a series of simple bacterial genetic manipulations, the frequency of repeating RGDS cell-adhesive ligands can be tuned without altering the other molecular-level design parameters. Additionally, a variety of other known cell-binding domains that have been incorporated into protein-engineered materials could also be designed into the MITCH gels to target specific cell interactions (61).

In summary, the use of WW and proline-rich peptide domains was demonstrated as an effective strategy to encapsulate multiple cell types within 3D hydrogels of tunable viscoelasticity. These materials undergo the sol-to-gel phase transition upon simple mixing of two polymers, thereby encapsulating cells at constant physiological conditions. Polymers with specific molecular-level design parameters were synthesized precisely by using protein engineering concepts to tailor the viscoelastic properties of the materials. The resulting hydrogels are shear-thinning, injectable, and self-healing, which may make them suitable for use in a wide range of experimental and clinical cell encapsulation applications.

Materials and Methods

Protein Engineering. The cloning scheme, primary sequence, and protein characterization are described in the *SI Materials and Methods*.

Particle Tracking. Microrheology used 0.2-μm tracer fluorescent particles (Molecular Probes) in buffer TN (100 mM Tris·HCl and 100 mM NaCl, pH 8.0) unless otherwise noted. After being mixed, 10-μL samples were pipetted immediately between a microscope slide and a coverslip separated by a 120-μm-thick SecureSeal Imaging Spacer (Grace Bio Labs). For shear-thinning, gels equilibrated 60 min in a syringe before ejection via a 26 gauge needle (5/8 in. in length, ≈0.42 mm in diameter; BD Biosciences). The Brownian dynamics of 20–50 beads were followed under a 40× oil-immersion objective, temporal resolution ≈30 Hz, for ≈15 s (iXON DV897 camera; Andor Technology). Stacks of images were analyzed following the methods and macros of Crocker and Grier (46) using IDL software, version 7.0.

Cell Encapsulation. Cells (5 μL, 20 × 10^6 cells per milliliter, HUVECs, PC-12 cells, or NSCs) were added first to C7 or N7 solution (5 μL) and then P9 (10 μL) on a glass coverslip. Cell viability was assessed with a LIVE/DEAD kit (Molecular Probes). Staining solution containing 2.0 μM calcein AM (λ_{ex} = 488 nm, λ_{em} = 515–540 nm) and 4.0 μM ethidium homodimer (λ_{ex} = 528 nm, λ_{em} = 560 nm) in PBS was incubated at 37 °C for 75 min and visualized by laser confocal microscopy. See *SI Materials and Methods* for details on culture maintenance and immunocytochemistry.

ACKNOWLEDGMENTS. We thank Nick Melosh, Megan Valentine, and Ian Wong for expertise and equipment for microrheology and Theo Palmer and Katrin Schrenk-Siemens for expertise in NSC culture. Work was supported by the National Heart Foundation (American Health Assistance Foundation H2007-024), John and Ulla de Larios Fund, and Stanford Bio-X Interdisciplinary Initiative. W.M. acknowledges a Stanford Graduate Fellowship; A.P.-A. acknowledges a National Science Foundation Graduate Fellowship.

1. Brandl F, Sommer F, Goepferich A (2007) Rational design of hydrogels for tissue engineering: Impact of physical factors on cell behavior. *Biomaterials* 28:134–146.
2. Beaty CE, Saltzman WM (1993) Controlled growth factor delivery induces differential neurite outgrowth in three-dimensional cell cultures. *J Control Release* 24:15–23.
3. Kim S, Healy KE (2003) Synthesis and characterization of injectable poly(*N*-isopropylacrylamide-*co*-acrylic acid) hydrogels with proteolytically degradable cross-links. *Biomacromolecules* 4:1214–1223.
4. Mahoney MJ, Anseth KS (2006) Three-dimensional growth and function of neural tissue in degradable polyethylene glycol hydrogels. *Biomaterials* 27:2265–2274.
5. Petka WA, Harden JL, McGrath KP, Wirtz D, Tirrell DA (1998) Reversible hydrogels from self-assembling artificial proteins. *Science* 281:389–392.
6. Shen W, Lammertink RGH, Sakata JK, Kornfield JA, Tirrell DA (2005) Assembly of an artificial protein hydrogel through leucine zipper aggregation and disulfide bond formation. *Macromolecules* 38:3909–3916.
7. Hennink WE, van Nostrum CF (2002) Novel crosslinking methods to design hydrogels. *Adv Drug Delivery Rev* 54:13–36.
8. Capito RM, Azevedo HS, Velichko YS, Mata A, Stupp SI (2008) Self-assembly of large and small molecules into hierarchically ordered sacs and membranes. *Science* 319:1812–1816.

9. Haines-Butterick L, et al. (2007) Controlling hydrogelation kinetics by peptide design for three-dimensional encapsulation and injectable delivery of cells. *Proc Natl Acad Sci USA* 104:7791–7796.
10. Pochan DJ, et al. (2003) Thermally reversible hydrogels via intramolecular folding and consequent self-assembly of a de novo designed peptide. *J Am Chem Soc* 125:11802–11803.
11. Niece KL, Hartgerink JD, Donners JJ, Stupp SI (2003) Self-assembly combining two bioactive peptide-amphiphile molecules into nanofibers by electrostatic attraction. *J Am Chem Soc* 125:7146–7147.
12. Gillette BM, et al. (2008) In situ collagen assembly for integrating microfabricated three-dimensional cell-seeded matrices. *Nat Mater* 7:636–640.
13. Wang S, Nagrath D, Chen PC, Berthiaume F, Yarmush ML (2008) Three-dimensional primary hepatocyte culture in synthetic self-assembling peptide hydrogel. *Tissue Eng Part A* 14:227–236.
14. Kuo CK, Ma PX (2008) Maintaining dimensions and mechanical properties of ionically crosslinked alginate hydrogel scaffolds in vitro. *J Biomed Mater Res A* 84:899–907.
15. Teixeira AI, Duckworth JK, Hermanson O (2007) Getting the right stuff: Controlling neural stem cell state and fate in vivo and in vitro with biomaterials. *Cell Res* 17:56–61.
16. Cao F, et al. (2007) In vivo imaging and evaluation of different biomatrices for improvement of stem cell survival. *J Tissue Eng Regen Med* 1:465–468.
17. Laflamme MA, et al. (2007) Cardiomyocytes derived from human embryonic stem cells in pro-survival factors enhance function of infarcted rat hearts. *Nat Biotechnol* 25:1015–1024.
18. Bjorklund A, et al. (2000) Towards a neuroprotective gene therapy for Parkinson's disease: Use of adenovirus, AAV and lentivirus vectors for gene transfer of GDNF to the nigrostriatal system in the rat Parkinson model. *Brain Res* 886:82–98.
19. Macias MJ, Gervais V, Civera C, Oschkinat H (2000) Structural analysis of WW domains and design of a WW prototype. *Nat Struct Biol* 7:375–379.
20. Macias MJ, Wiesner S, Sudol M (2002) WW and SH3 domains, two different scaffolds to recognize proline-rich ligands. *FEBS Lett* 513:30–37.
21. Kanelis V, Rotin D, Forman-Kay JD (2001) Solution structure of a Nedd4 WW domain–ENaC peptide complex. *Nat Struct Biol* 8:407–412.
22. Russ WP, Lowery DM, Mishra P, Yaffe MB, Ranganathan R (2005) Natural-like function in artificial WW domains. *Nature* 437:579–583.
23. Socolich M, et al. (2005) Evolutionary information for specifying a protein fold. *Nature* 437:512–518.
24. de Jong SJ, van Eerdenbrugh B, van Nostrum CF, Kettenes-van den Bosch JJ, Hennink WE (2001) Physically crosslinked dextran hydrogels by stereocomplex formation of lactic acid oligomers: Degradation and protein release behavior. *J Control Release* 71:261–275.
25. Lim DW, Park TG (2000) Stereocomplex formation between enantiomeric PLA-PEG triblock copolymers: Characterization and use as protein-delivery microparticulate carriers. *J Appl Physiol* 75:1615–1623.
26. Koopmans C, Ritter H (2008) Formation of physical hydrogels via host-guest interactions of β-cyclodextrin polymers and copolymers bearing adamantyl groups. *Macromolecules* 41:7418–7422.
27. van de Manakker F, et al. (2008) Self-assembling hydrogels based on β-cyclodextrin/cholesterol inclusion complexes. *Macromolecules* 41:1766–1773.
28. Yamaguchi N, et al. (2007) Growth factor mediated assembly of cell receptor-responsive hydrogels. *J Am Chem Soc* 129:3040–3041.
29. Seal BL, Panitch A (2003) Physical polymer matrices based on affinity interactions between peptides and polysaccharides. *Biomacromolecules* 4:1572–1582.
30. Topp S, Prasad V, Cianci GC, Weeks ER, Gallivan JP (2006) A genetic toolbox for creating reversible Ca^{2+}-sensitive materials. *J Am Chem Soc* 128:13994–13995.
31. Shapiro AM, et al. (2000) Islet transplantation in seven patients with type 1 diabetes mellitus using a glucocorticoid-free immunosuppressive regimen. *N Engl J Med* 343:320–328.
32. Rafii S, Lyden D (2003) Therapeutic stem and progenitor cell transplantation for organ vascularization and regeneration. *Nat Med* 9:702–712.
33. Bliss T, Guzman R, Daadi M, Steinberg GK (2007) Cell transplantation therapy for stroke. *Stroke* 38:817–826.
34. Willerth SM, Sakiyama-Elbert SE (2008) Cell therapy for spinal cord regeneration. *Adv Drug Delivery Rev* 60:263–273.
35. Straley KS, Wong Po Foo C, Heilshorn S (2009) Biomaterial design strategies for the treatment of spinal cord injuries. *J Neurotrauma*, 10.1089/neu.2009/0948.
36. Nakagomi N, et al. (2009) Endothelial cells support survival, proliferation and neuronal differentiation of transplanted adult ischemia-induced neural stem/progenitor cells after cerebral infarction. *Stem Cells* 27:2185–2195.
37. Ziv Y, Avidan H, Pluchino S, Martino G, Schwartz M (2006) Synergy between immune cells and adult neural stem/progenitor cells promotes functional recovery from spinal cord injury. *Proc Natl Acad Sci USA* 103:13174–13179.
38. Bliss TM, et al. (2006) Transplantation of hNT neurons into the ischemic cortex: Cell survival and effect on sensorimotor behavior. *J Neurosci Res* 83:1004–1014.
39. Kelly S, et al. (2004) Transplanted human fetal neural stem cells survive, migrate, and differentiate in ischemic rat cerebral cortex. *Proc Natl Acad Sci USA* 101:11839–11844.
40. Saporta S, Borlongan CV, Sanberg PR (1999) Neural transplantation of human neuroteratocarcinoma (hNT) neurons into ischemic rats. A quantitative dose–response analysis of cell survival and behavioral recovery. *Neuroscience* 91:519–525.
41. Kordower JH, et al. (1998) Fetal nigral grafts survive and mediate clinical benefit in a patient with Parkinson's disease. *Mov Disord* 13:383–393.
42. Kordower JH, et al. (1995) Neuropathological evidence of graft survival and striatal reinnervation after the transplantation of fetal mesencephalic tissue in a patient with Parkinson's disease. *N Engl J Med* 332:1118–1124.
43. Huang X, et al. (2000) Structure of a WW domain containing fragment of dystrophin in complex with β-dystroglycan. *Nat Struct Biol* 7:634–638.
44. McGrath KP, Fournier MJ, Mason TL, Tirrell DA (1992) Genetically directed syntheses of new polymeric materials. Expression of artificial genes encoding proteins with repeating -$(AlaGly)_3$ProGluGly- elements. *J Am Chem Soc* 114:727–733.
45. Chen DT, et al. (2003) Rheological microscopy: Local mechanical properties from microrheology. *Phys Rev Lett* 90:108301.
46. Crocker JC, Grier DG (1996) Methods of digital video microscopy for colloidal studies. *J Colloid Interface Sci* 179:298–310.
47. Flory PJ (1941) Molecular size distributions in three dimensional polymers. I. Gelation. *J Am Chem Soc* 63:3083–3090.
48. Stockmayer WH (1943) Theory of molecular size distribution and gel formation in branched-chain polymers. *J Chem Phys* 11:45–55.
49. Semenov AN, Rubinstein M (1998) Thermoreversible gelation in solutions of associative polymers. I. Statics. *Macromolecules* 31:1373–1385.
50. Discher DE, Janmey P, Wang YL (2005) Tissue cells feel and respond to the stiffness of their substrate. *Science* 310:1139–1143.
51. Ghosh K, Ingber DE (2007) Micromechanical control of cell and tissue development: Implications for tissue engineering. *Adv Drug Delivery Rev* 59:1306–1318.
52. Janmey PA, McCulloch CA (2007) Cell mechanics: Integrating cell responses to mechanical stimuli. *Annu Rev Biomed Eng* 9:1–34.
53. Wirtz D (2009) Particle-tracking microrheology of living cells: Principles and applications. *Annu Rev Biophys* 38:301–326.
54. Zaman MH, et al. (2006) Migration of tumor cells in 3D matrices is governed by matrix stiffness along with cell-matrix adhesion and proteolysis. *Proc Nat Acad Sci USA* 103:10889–10894.
55. Straley KS, Heilshorn SC (2009) Independent tuning of multiple biomaterial properties using protein engineering. *Soft Matter* 5:114–124.
56. Babu H, Cheung G, Kettenmann H, Palmer TD, Kempermann G (2007) Enriched monolayer precursor cell cultures from micro-dissected adult mouse dentate gyrus yield functional granule cell-like neurons. *PLoS One* 2:e388.
57. Niece KL, et al. (2008) Modification of gelation kinetics in bioactive peptide amphiphiles. *Biomaterials* 29:4501–4509.
58. Saha K, et al. (2008) Substrate modulus directs neural stem cell behavior. *Biophys J* 95:4426–4438.
59. Byfield FJ, Reen RK, Shentu TP, Levitan I, Gooch KJ (2009) Endothelial actin and cell stiffness is modulated by substrate stiffness in 2D and 3D. *J Biomech* 42:1114–1119.
60. Pedersen JA, Swartz MA (2005) Mechanobiology in the third dimension. *Ann Biomed Eng* 11:1469–1490.
61. Straley KS, Heilshorn SC (2009) Design and adsorption of modular engineered proteins to prepare customized, neuron-compatible coatings. *Front Neuroengineering* 2:9.